

---

# PipeFusion: Displaced Patch Pipeline Parallelism for Inference of Diffusion Transformer Models

---

**Jiannan Wang\***  
Tencent & The University of Hong Kong  
steaunkwang@tencent.com

**Jiarui Fang\*†**  
Tencent  
jiaruifang@tencent.com

**Aoyu Li**  
Tencent  
aoyuli@tencent.com

**Pengcheng Yang**  
Tencent  
apcyang@tencent.com

## Abstract

This paper introduces PipeFusion, a novel approach that harnesses multi-GPU parallelism to address the high computational and latency challenges of generating high-resolution images with diffusion transformers (DiT) models. PipeFusion splits images into patches and distributes the network layers across multiple devices. It employs a pipeline parallel manner to orchestrate communication and computations. By leveraging the high similarity between the input from adjacent diffusion steps, PipeFusion eliminates the waiting time in the pipeline by reusing the one-step stale feature maps to provide context for the current step. Our experiments demonstrate that it can generate higher image resolution where existing DiT parallel approaches meet OOM. PipeFusion dramatically cuts communication bandwidth, allowing DiT inference to run on PCIe-linked GPUs instead of expensive NVLink setups. This paves the way for the deployment of DiT inference on a very large scale. Our code is publicly available at <https://github.com/PipeFusion/PipeFusion>.

## 1 Introduction

The ability of AI-generated content (AIGC) is rapidly growing. With the advent of breakthroughs like OpenAI’s Sora [1], we are transitioning from the era of image generation to video generation. Diffusion models [2], a leading generative technique, have solidified their role as the preferred method for both image and video synthesis. To generate high-resolution images and long-time-span high-fidelity videos, diffusion models require further enhancement. Currently, we are observing a significant shift in the foundational network architecture of these models. There is a migration taking place from the traditional U-Net [3] to Diffusion Transformers (DiTs) [4], due to their increased model capacity and scalability. Concurrently, the spatial shape of generation content from diffusion models is growing larger, which is crucial for processing lengthy videos and detailed images.

The inference latency of generating long visual sequences from DiT models is notably high due to the quadratic growth in computation time with the sequence length because of the attention mechanism. It has been reported that the inference latency of Sora, a variant of DiT, can reach several minutes. Given that a single GPU cannot satisfy the latency requirements for practical applications, it becomes necessary to parallelize the DiT inference for a single image across multiple computational devices. However, parallelization techniques commonly used in large language models (LLMs), such as tensor parallelism [5] and sequence parallelism [6, 7], prove to be inefficient for diffusion models due to

---

\*Indicates equal contributions. Work is done when Jiannan Wang is an intern at Tencent.

†Corresponding author

their large activation sizes. In such cases, the communication costs often outweigh the benefits of parallel computation. Consequently, the deployment of DiT still requires GPU clusters equipped with high-bandwidth interconnects, such as NVLink.

Some studies have focused on leveraging the special characteristics of diffusion models to speed up parallel inference [8, 9]. DistriFusion [9] observed a high degree of similarity in both inputs and activations across successive diffusion time steps, a phenomenon we refer to as **input temporal redundancy**. DistriFusion introduced a patch parallelism strategy, wherein the input image is segmented into patches, and each computational device is tasked with generating a specific patch. By capitalizing on the input temporal redundancy, this approach utilizes local fresh activations in conjunction with one-step stale activations to engage in cross-attention and convolution operations within the U-Net-based diffusion model SDXL [10]. This technique effectively hides communication costs with the computation of a diffusion step. Nonetheless, when this method is applied to DiT, it comes at the cost of inefficient memory usage. DistriFusion maintains a full spatial shape of attention key (K) and value (V) for all layers. The memory overhead does not diminish with an increase in the number of computational devices, posing a scalability challenge.

We discover a more efficient parallel approach named PipeFusion that takes advantage of input temporal redundancy. As shown in Figure 1, PipeFusion distributes the DiT network across layers onto multiple devices, with each device managing several DiT layers, and segments the input images into multiple patches. PipeFusion orchestrates computation and communication in a pipeline manner and employs asynchronous P2P on activations across two adjacent devices. The method is applied to a single image, different from pipeline parallelism [11, 12] works on the batch dimension, and given the typically large number of diffusion steps, the pipeline’s idle time becomes negligible. In contrast to DistriFusion, PipeFusion dramatically decreases the volume of data communicated and the memory footprint. It solely transfers the input activation of the initial layer and the output activation of the final layer on each device, while DistriFusion conducts collective communication of activations, encompassing attention keys and values, for every DiT layer. This substantial reduction in communication volume correspondingly diminishes the memory buffer required for asynchronous communication. PipeFusion effectively removes the need for high hardware bandwidth in DiT model inference. Our experimental results indicate that the DiT inference latency on PCIe machines is on par with that on NVLink machines, as we have almost entirely eliminated the communication overhead.

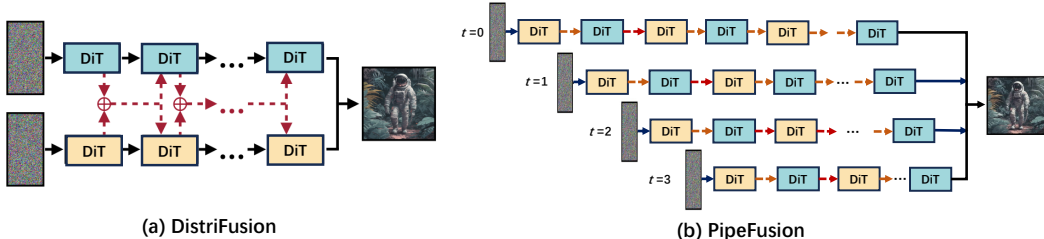


Figure 1: (a) DistriFusion replicates DiT parameters on two devices. It splits an image into 2 patches and employs asynchronous allgather for activations of every layer. (b) PipeFusion shards DiT parameters on two devices. It splits an image into 4 patches and employs asynchronous P2P for activations across two devices.

## 2 Background & Related Works

**Diffusion Models:** To generate a high-quality image, diffusion models often utilize a noise-prediction deep neural network (DNN), commonly employing U-Net [3] and Diffusion Transformers (DiT) [4] as backbones, denoted by  $\epsilon_\theta$ . The process starts from pure Gaussian noise  $x_T \sim \mathcal{N}(0, I)$  and involves numerous iterative denoising steps to produce the final meaningful image  $x_0$ , with  $T$  representing the total number of diffusion time steps. Specifically, at each diffusion time step  $t$ , given the noisy image  $x_t$ , the model  $\epsilon_\theta$  takes  $x_t$ ,  $t$ , and an additional condition  $c$  (e.g., text, image) as inputs to predict the corresponding noise  $\epsilon_t$  within  $x_t$ . At each denoising step, the previous image  $x_{t-1}$  can be obtained from the following equation:

$$x_{t-1} = \text{Update}(x_t, t, \epsilon_t), \quad \epsilon_t = \epsilon_\theta(x_t, t, c). \tag{1}$$

In this context, Update denotes a function that is specific to the sampler, i.e. DDIM [2], and generally involves operations such as element-wise operations. Consequently, the predominant contributor to diffusion model inference latency is attributed to the forward propagation through the model  $\epsilon_\theta$ . The architecture of diffusion model  $\epsilon_\theta$  is undergoing a pivotal transition from U-Net [3] to Diffusion Transformers (DiT) [13, 14], driven by the scaling law that links increased model parameters with enhanced capabilities. As diffusion models tackle higher-resolution images and longer visual sequences, it imposes a quadratic computational burden on these models, which escalates the latency for generating high-resolution images, making it impractical for real-world use. Consequently, there is an urgent need to develop parallel processing techniques to mitigate the inference latency associated with diffusion models.

From the algorithmic perspective, efforts to accelerate the diffusion model inference include compression to latent space [15, 16], improving sampling algorithms [17–20], and model distillation [21, 22]. This paper focuses on efficiently parallelizing transformer-based diffusion models, which can be used orthogonally with the above methods.

**Transformers Parallelism:** The attention mechanism of transformers requires each position in the input to attend to all positions, therefore a naive approach of splitting an image into  $N$  patches across  $N$  devices, with each device individually processing its own patch, fails to yield accurate generative outcomes [9]. Considering DiT’s affinity to Large Language Models (LLMs), both tensor parallelism [5] and sequence parallelism [6, 7], which are commonly utilized for efficient inference in LLMs, can be adapted for DiT. Nevertheless, diffusion models have longer sequence lengths and smaller model sizes, yet the communication overhead remains substantial during inference. These methods impose high bandwidth and memory requirements on inference devices. DistriFusion [9] introduced displaced patch parallelism for U-Net diffusion models, which divides the model’s input into multiple patches and facilitates the asynchronous communication of activations and communication overlaps with computation. However, when applying the method to the DiTs the cost of the memory buffer leads to a huge memory cost. In summary, the current parallel approaches of diffusion models rely on high-bandwidth inter-GPU bandwidth via NVLink to achieve effective scalability. This often requires the use of expensive A100 or even H100 clusters, which contributes to the persistently high inference costs associated with DiTs.

This work leverages the observed similarity of inputs between adjacent diffusion steps and also divides the image into patches. However, we organize the computation and communication into a pipeline parallel manner. Our approach is different from the other pipeline parallel approaches [11, 12], which often rely on a batch of inputs and splitting the batch dimension for micro-batching to achieve streaming computation. The work divides the workload of a single image inference and does not depend on the batch dimension.

### 3 Methods

In this section, we conduct a systematic study of parallel approaches for the DiT Model inference. Initially, we highlight the potential to apply tensor parallelism and sequence parallelism from LLM to DiT. Then, we investigate applying dispatched patch parallelism proposed in DistriFusion from U-Net diffusion models to DiT. Finally, we introduce our proposed method, which offers superior communication and memory efficiency compared to the above approaches.

Table 1: Comparison of Different Parallelism for DiT for a single diffusion step (\* indicates asynchronous communication)

	attn-KV	communication cost	param	Memory	
				QO Activations	KV Activations
Tensor Parallel	fresh	$4O(p \times hs)L$	$\frac{1}{N}P$	$\frac{2}{N}A = \frac{1}{N}QO$	$\frac{2}{N}A = \frac{1}{N}KV$
DistriFusion*	stale	$2O(p \times hs)L$	$P$	$\frac{2}{N}A = \frac{1}{N}QO$	$2AL = (KV)L$
Ring Seq Parallel*	fresh	NA	$P$	$\frac{2}{N}A = \frac{1}{N}QO$	$\frac{2}{N}A = \frac{1}{N}KV$
Ulysses Seq Parallel	fresh	$4O(p \times hs)L$	$P$	$\frac{2}{N}A = \frac{1}{N}QO$	$\frac{2}{N}A = \frac{1}{N}KV$
PipeFusion*	stale-	$2O(p \times hs)$	$\frac{1}{N}P$	$\frac{2}{M}A = \frac{1}{M}QO$	$\frac{2L}{N}A = \frac{1}{N}(KV)L$

Table 1 compares the memory and communication performance of different DiT parallel approaches. In the table,  $p$  represents the generation visual sequence length (pixels in latent space), and  $hs$  denotes

the hidden size of the model.  $L$  stands for the number of network layers,  $P$  is the total number of parameters. The parameter number of the query ( $Q$ ), key ( $K$ ), value ( $V$ ), and output ( $O$ ) activation of the attention module is the same, which is  $A$  in the Table. The peak activation memory cost is the same as the cost of a single attention layer which mainly consist of  $Q, O, K, V$  activations. In the column of attn-KV, fresh indicates using the KV of the current diffusion step, while stale refers to using a part of the KV from the previous diffusion step. The \* after name indicates it employs asynchronous communication, and the communication cost can be hidden by computation.

### 3.1 Sequence Parallelism & Tensor Parallelism

Considering the similarity in network architectures, tensor parallelism (TP) [5] and sequence parallelism (SP) [6, 7] proposed for LLM can be applied to DiT inference. The primary components of both DiT and LLM consist of Multi-Head Self-Attention followed by a Feed-Forward Network (FFN). Tensor parallelism can be applied to transformer inference by partitioning the weight tensors in a way specifically designed for transformers. As depicted in Table 1, tensor Parallelism can reduce memory usage of both parameters and activations to  $\frac{1}{N}$ . It requires two synchronous all-reduce operations afterward the attention and FFN modules, which brings  $4O(p \times hs)$  for each layer. To utilize sequence parallelism, we can split the input images into patches, and the multi-head attention module in DiT can employ Ring-Attention [7], or DeepSpeed-Ulysses [6], or a combination of both [23]. The Ulysses sequence parallelism requires 4 all-to-all operations and brings a  $4O(p \times hs)$  for each layer, which is the same as tensor parallelism. Ring-attention is another sequence parallel paradigm that can hide K, V transmission with computation inside the attention module. Tensor parallelism and sequence parallelism can be combined in a hybrid way in DiT inference.

### 3.2 Displaced Patch Parallelism

Diffusion Model inference, distinct from LLM inference, consists of multiple steps. It is observed the high degree of similarity observed in the inputs and activations across successive diffusion time steps [9]. We term this phenomenon *input temporal redundancy*. This redundancy implies that the computation for an activation patch in a given layer does not exclusively hinge on the latest activations of other patches. It is viable to incorporate slightly outdated (stale) activations from the previous diffusion step. By blending these stale activations with a fraction of newly computed activations, we can still produce accurate final generation results.

By taking advantage of this feature, DistriFusion proposed *displaced patch parallelism*. The method partitions an input image into  $N$  patches, where  $N$  is the number of devices, assigning each computing device the task of computing the output results for its respective patch. However, operators like convolution and attention necessitate the exchange of intermediate activations among patches. Specifically, the self-attention modules of DiT require K and V activations with a full spatial shape. It uses asynchronous all-gather to collect K, and V activations of the previous diffusion step, and compute with one step stale K, and V activations simultaneously.

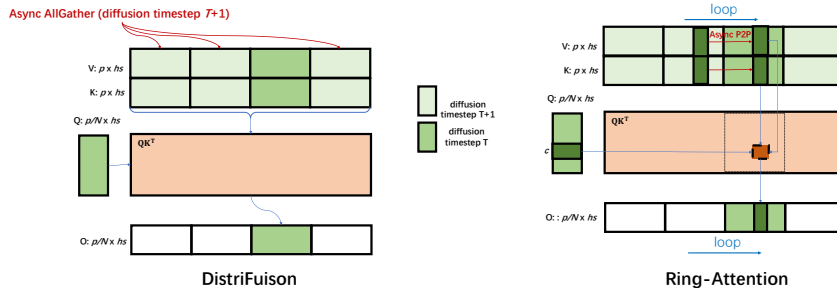


Figure 2: The DistriFusion vs. Sequence Parallelism of Ring-Attention for an Attention Module.

DistriFusion can be considered a form of asynchronous sequence parallelism. It hides the KV communication with forward computation of a diffusion step, at the cost of more memory consumption. We compare DistriFusion and sequence parallelism of Ring-Attention in Figure 2, both of which employ asynchronous communication and splitting images into patches. As shown in the left part

of Figure 2, DistriFusion leverages a fraction  $\frac{N-1}{N}$  of the activation  $K, V$  from timestep  $T+1$  in conjunction with a fraction  $\frac{1}{N}$  of the local  $KV$  at timestep  $T$ , compute attention operation with the local queries at diffusion timestep  $T$ . The communication of  $K, V$  at timestep  $T$  is designed to be overlapped with the network forward computation for timestep  $T$ . As shown in the right part of Figure 2, Ring-Attention [7] achieves fine-grained overlap of communication and computation within the attention module and uses the fresh  $K, V$ . Leveraging input temporal redundancy, DistriFusion can more effectively hide communication overhead compared to Ring-Attention, as it allows  $KV$  communication to overlap with the entire forward computation of a diffusion step, whereas Ring-Attention only permits communication overlap within the attention module itself. However, a drawback of DistriFusion is to maintain a large communication buffer. In the Ring-Attention, its communication buffer of  $c \times hs$  can be controlled by the block size  $c$  in the figure, which is a value smaller than  $\frac{L}{N}$ . DistriFusion requests that each computational device always maintains communication buffers of the full spatial shape of the  $KVs$ , which is  $AL$  in total. In other words, the memory cost of DistriFusion does not decrease with the addition of computational devices.

### 3.3 Displaced Patch Pipeline Parallelism

We have proposed a pipelined parallel approach named PipeFusion, which more effectively leverages the input temporal redundancy. This approach surpasses DistriFusion by offering increased memory efficiency and reduced communication costs. Additionally, PipeFusion can achieve higher accuracy than DistriFusion.

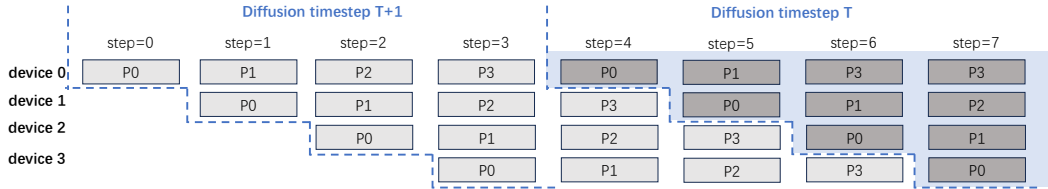


Figure 3: The Workflow of Displaced Patch Pipeline Parallelism.

PipeFusion partitions an input image into  $M$  non-overlapping patches. The DiT network is partitioned into  $N$  stages ( $N < L$ ), which are sequentially assigned to  $N$  computational devices. Note that  $M$  and  $N$  can be unequal, which is different from the image-splitting approaches used in sequence parallelism and DistriFusion. Each device processes the computation task for one patch of its assigned stage in a pipelined manner. It is advantageous for the workload of the denoiser network to be evenly partitioned into  $N$  segments. This works well with DiT models because they have many identical blocks of transformers that repeat. However, the U-Net Diffusion Model doesn't have this kind of repeating structure.

The example in Figure 3 demonstrates the pipeline workflow for two diffusion steps with  $N = 4$  and  $M = 4$ , where the computations for timestep  $T + 1$  (light grey) are completed before those for timestep  $T$  (dark grey). Patch P0 (Patch 0) is computed on device 0, then passed to device 1, while device 0 computes P1 (Patch 1) in parallel. Since the computations of a sampler are element-wise operations, all of the diffusion steps can be pipelined. Leveraging input temporal redundancy, a device does not need to wait for the receiving of full spatial shape activations for the current pipeline step to start the computation of its own stage. Instead, it employs the one-step stale activations to provide context for the current step. Consequently, after the pipeline is initialized, there is no waiting time within the pipeline. Considering the pipeline bubble, the effective computation ratio of the pipeline is  $\frac{M \cdot S}{M \cdot S + N - 1}$ , where  $S$  is the number of diffusion timesteps. Due to the large number of diffusion steps, the effective computation ratio is high. For example, with  $M = N = 4$  and  $S = 50$ , the effective computation ratio is 98.5%.

As evidenced in Table 1, PipeFusion demonstrates superior efficiency in both communication and memory usage. It transmits between computational devices only the activations that serve as inputs and outputs for a series of consecutive transformer layers belonging to a stage. The communication cost is  $2O(p \times hs)$ , which is not associated with the term  $L$ . It significantly reduces the communication bandwidth requirements in comparison to other methods that transmits  $K$  and  $V$  activations for  $L$  layers. Furthermore, PipeFusion hides communication within the computation by using asynchronous

P2P transfers of previous step Patch data and reception of subsequent step Patch data to overlap with the current Patch computation. For example, during step 4, device 0 receives data for  $P_1$  of diffusion step  $T$  while concurrently computing  $P_0$  of the same step  $T$ . Similarly, the transmission of  $P_0$  for diffusion step  $T$  can be hidden with the computation of  $P_1$  for diffusion step  $T$  at step 5. Regarding memory efficiency, each device in the PipeFusion setup stores only  $\frac{1}{N}$  of the parameters relevant to its specific stage. Since the use of stale KV for attention computation requires that each device maintains the full spatial KV for its corresponding  $\frac{L}{N}$  layers of its stage, this overhead is significantly smaller than that of DistriFusion and diminishes as the number of devices increases. This approach is markedly more memory-efficient than alternative methods in the table.

In terms of the final generated image accuracy, PipeDiffusion theoretically outperforms DistriFusion because it utilizes more fresh activations. We label the "-" after stable for PipeFusion in Table 1, indicating its stableness is better than DistriFusion. As shown in Figure 4, within a single diffusion step, PipeDiffusion continuously increases the area of fresh activation as the pipeline steps progress at diffusion step  $T$  and  $M=4$ . In contrast, DistriFusion maintains a constant fresh area of one patch, which is  $\frac{1}{N}$ , throughout the entire diffusion step. It deserves to be emphasized that the precision preservation design of DistriFusion for the group normalization layers in U-Net, specifically the *Corrected Asynchronous GroupNorm*, can be seamlessly applied in PipeFusion, although DiT does not employ group norm layer.

The use of input temporal redundancy requires a warmup period because the behavior of diffusion synthesis undergoes qualitative changes throughout the denoising process. Therefore, DistriFusion incorporates several warm-up steps of standard synchronous patch parallelism as a preliminary phase. For DistriFusion, warmup cannot be executed in a pipelined manner and will introduce pipeline bubbles. However, considering the relatively low proportion of warmup steps, the impact on performance is limited. To optimize the warmup overhead, the warmup steps can be separated from the remaining steps and allocated to different computational resources.

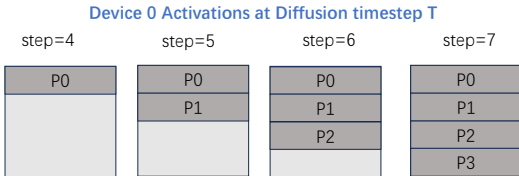


Figure 4: The fresh part of activations during diffusion timestep  $T$ . The dark gray represents fresh data and the light gray represents stable data.

## 4 Experiments

### 4.1 Setups

**Models:** Our method requires off-the-shelf pretrained diffusion transformers. We conduct our experiments on Pixart- $\alpha$  [24] (0.6B). It supports high-resolution image synthesis up to 1024px resolution. It employs a standard DiT [4] and incorporates cross-attention modules to inject text conditions.

**Hardware:** Three GPU clusters are used for our evaluation, including a 4xGPU A100 80GB (PCIe) cluster, an 8xGPU A100 80GB (NVLink) cluster, and an 8xGPU L20 40GB (PCIe) cluster. The measured GPU P2P bandwidth is 23 GB/s, 268 GB/s and 26 GB/s, respectively.

**Software:** We compare our PipeFusion against the following baselines in terms of both quality and efficiency. We pick the best latency performance by searching patch number  $M$  from 2, 4, 8, 16, 32. **Tensor Parallelism:** we implement a tensor parallelism DiT referring to Megatron-LM; **Sequence Parallelism:** we apply two different sequence parallelism, i.e. DeepSpeed-Ulysses and Ring-Attention; **DistriFusion:** We adapt the official DistriFusion [25] from U-Net Diffusion Model to DiT; **Original:** a serial implementation on a single GPU. Our software is built using PyTorch 2.3.0 and huggingface diffusers 0.27.2 and flash-attn 2.5.8.

We observe a memory spike in the VAE (Variational Autoencoder) due to temporary memory usage in convolution operators. This results in the VAE requiring significantly more memory than the DiT layers. To mitigate this issue, we have implemented a strategy where the input image to convolutional layers is divided into several chunks, transforming a single convolution operation into a sequence

of multiple operations executed in order, thereby avoiding the temporary memory spike, similar to work [26]. The checkpoint is downloaded from huggingface [27].

## 4.2 Results

### 4.2.1 Quality results

In Figure 5, we show some qualitative visual results. The images produced by PipeFusion are virtually indistinguishable from the original images to the human eye, on various settings of the number of patches or the number of devices. When the patch number is 1, PipeFusion achieves equivalent accuracy to DistriFusion. As the patch number exceeds 1, its accuracy approaches that of the original version more closely than PipeFusion theoretically. Additionally, we include the Fréchet Inception Distance (FID) [28] in the figure, which indicates that PipeFusion slightly outperforms DistriFusion in terms of FID on the same device, with a lower FID score being preferable. We use 20-Step DPM-Solver and the warmup step is 4 for DistrFusion and DistriPipeline.

### 4.2.2 Latency & Memory

To evaluate the latency and memory performance, we scale image generation resolution on Pixart- $\alpha$  from 1024px to 8192px, on three GPU clusters. We use 20-Step DPM-Solver and the warmup step is 1 for DistrFusion and DistriPipeline.

On the 4x A100 (PCIe) cluster, we present the memory utilization in Figure 7 and the end-to-end latency in Figure 6. Our proposed method, PipeFusion, demonstrates superior performance in terms of latency, particularly for the 1024px, 2048px, and 8192px scenarios. Specifically, PipeFusion achieves a latency reduction of 2.01x, 1.48x, and 1.10x compared to the best results obtained by other parallelization techniques, respectively. For the 4096px scenario, although PipeFusion is not the best one, it nonetheless demonstrates a remarkably close latency performance, being only 0.97x that of the sequence parallelism with DeepSpeed-Ulysses. Furthermore, PipeFusion delivers significant speedups of 3.1x and 2.4x over the baseline single-GPU performance for image generation tasks at resolutions ranging from 1024px to 8192px. In terms of memory efficiency, PipeFusion generally surpasses other methods, except tensor parallelism. It is worth noting that while tensor parallelism maintains the lowest memory footprint, as corroborated by the analysis in Table 1, it incurs higher latency compared to other parallelization strategies. Notably, for the 8192px case, both DistriFusion and sequence parallelism encounter out-of-memory (OOM) issues.

On the 8xL20 (PCIe) cluster, the latency performance of various methods is depicted in Figure 8. PipeFusion exhibits the lowest latency for the 1024px and 4096px scenarios, outperforming the best results of other parallel approaches by 1.47x and 1.31x, respectively. For the 2048px case, PipeFusion’s latency is nearly on par with DistriFusion, achieving a latency ratio of 0.99x. Both DistriFusion and sequence parallelism encounter out-of-memory (OOM) issues when tasked with generating images at the 4096px resolution. PipeFusion demonstrates significant speedups over the single GPU baseline performance, with a 2.46x improvement for the 1024px case and a substantial 4.3x speedup for the 4096px case.

On the 8xA100 (NVLink) cluster, while PipeFusion does not secure the lowest latency, it nonetheless demonstrates superior memory efficiency. Notably, both PipeFusion and tensor parallelism are capable of handling the demanding 8192px scenario, while DistriFusion and sequence parallelism (Ulysses) encounter OOM issues. For resolutions under 4192px, DistriFusion and sequence parallelism (Ulysses) manage to achieve the lowest latency. The NVLink’s high collective communication bandwidth diminishes the effectiveness of asynchronous communication. A notable observation is that the latency of sequence parallelism (Ulysses) using asynchronous communication closely resembles that of asynchronous DistriFusion, and it outperforms the Ring version. In addition, PixArt- $\alpha$  faces a limitation when deployed across eight devices, as the 28 DiT layers cannot be evenly partitioned among the eight GPUs, resulting in additional overhead.

In Figure 10(a), we compared the latency of the same task on A100 GPUs PCIe and NVLink clusters, to evaluate the impact of network bandwidth on latency. Across 1024px and 4096px cases, the latency of the PipeFusion on NVLink and PCIe are similar. Interestingly, PCIe even exhibits a slight advantage in speed. On PCIe cluster, PipeFusion is always faster than DistriFusion on the same task. **This demonstrates that PipeFusion’s communication bandwidth requirements are so minimal that they do not necessitate the application of a high-bandwidth network such as NVLink.** On

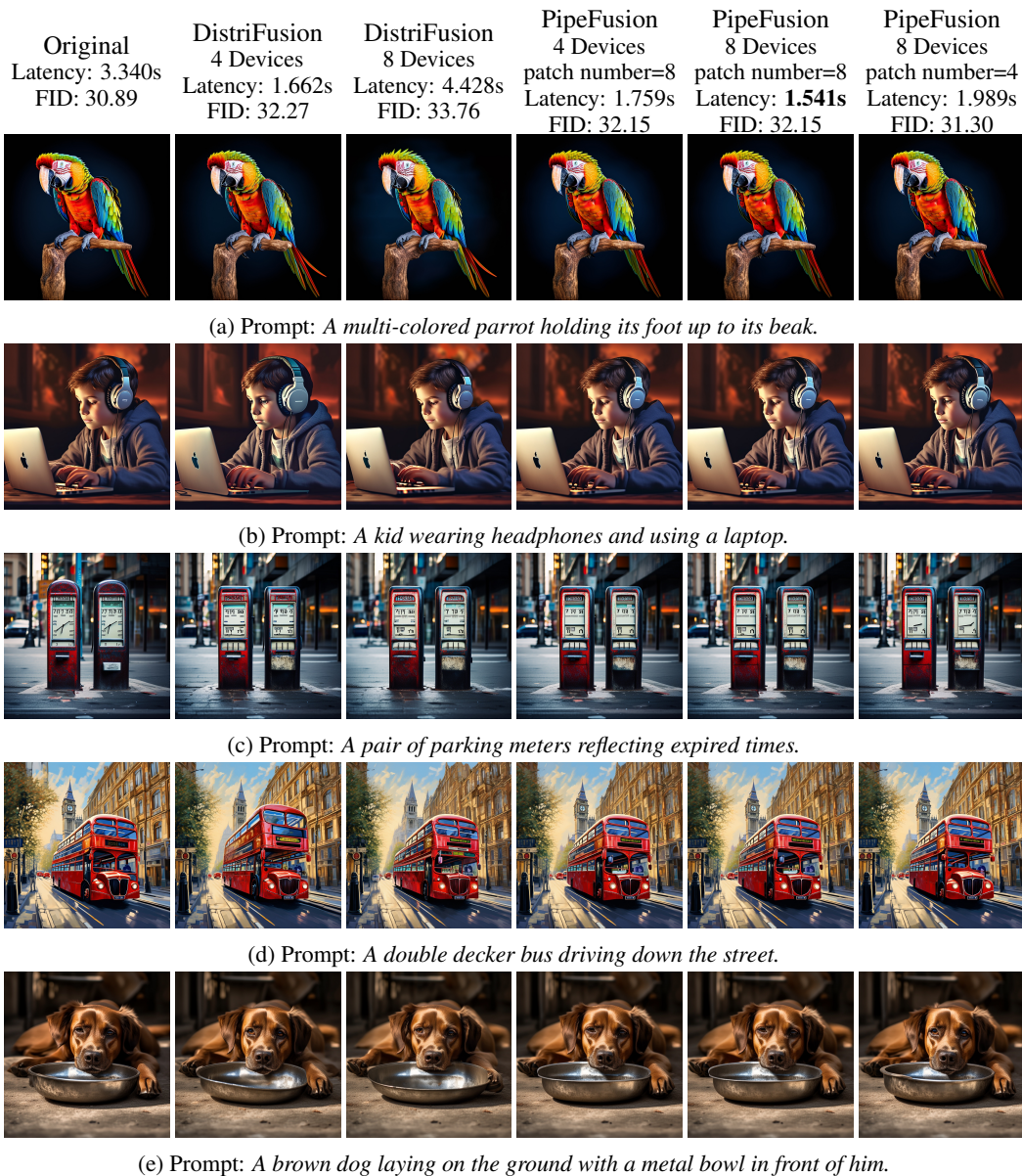


Figure 5: Qualitative results on L20(PCIE). FID is computed against the ground-truth images. We use the COCO Captions 2014 [29] dataset to benchmark these methods. For evaluation, a subset comprising 5,000 images is randomly sampled from the validation set to serve as the reference dataset. Concurrently, each experiment generates 5,000 images, each paired with a caption derived from the COCO Captions 2014 dataset, as the sample dataset. The quality of images generated by PipeFusion closely resembles that of the original images, regardless of whether 4 or 8 devices are used, and across varying patch numbers.



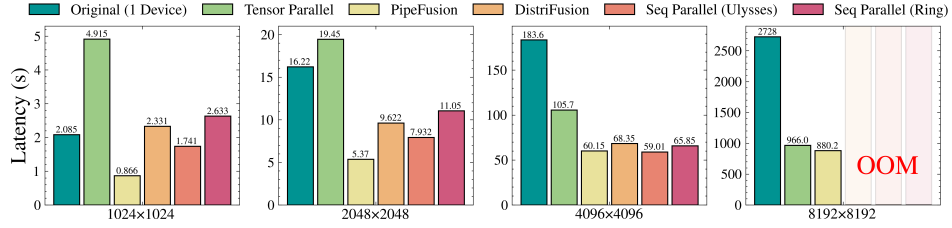


Figure 6: Overall Latency of Various Approaches for Pixart- $\alpha$  Image Generation Tasks Across Four Resolutions Using the 20-Step DPM-Solver on a 4×A100-80GB (PCIe).

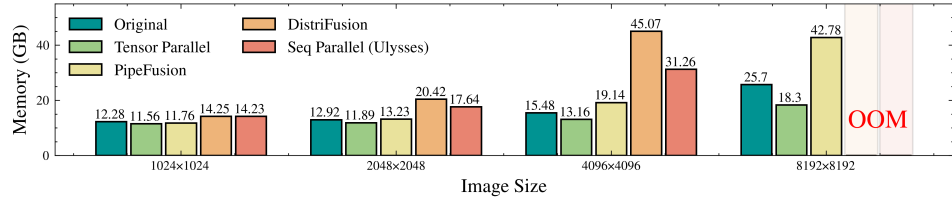


Figure 7: Max GPU Memory of Various Approaches for Pixart- $\alpha$  Image Generation Tasks Across Four Resolutions Using the 20-Step DPM-Solver on a 4×A100-80GB (PCIe).

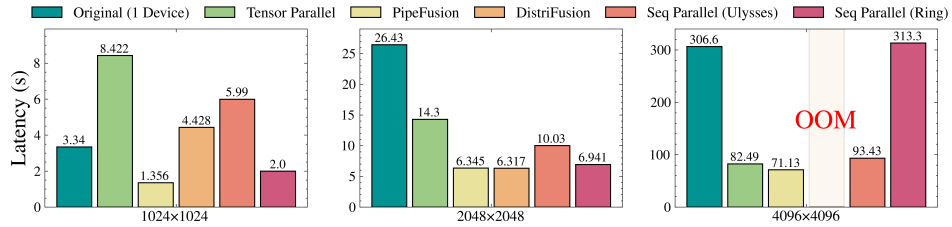


Figure 8: Overall latency on Pixart- $\alpha$  of various parallel approaches on three image generation tasks with the 20-Step DPM-Solver on 8×L20(PCIe).

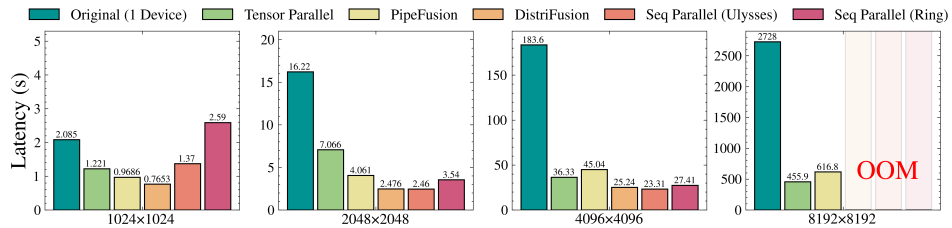


Figure 9: Overall latency on Pixart- $\alpha$  of various parallel approaches on three image generation tasks with the 20-Step DPM-Solver on 8×A100(NVLink).

NVLink Cluster, For the 1024px case, DistriFusion exhibits poor scalability from 4 GPUs to 8 GPUs; however, its scalability is better at 4096px. This is because higher-resolution tasks have a higher computational proportion, which makes them more amenable to scaling on the NVLink network.

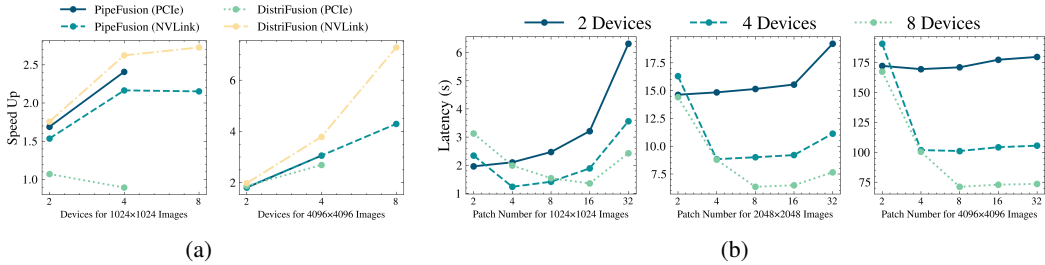


Figure 10: (a) Scalability of PipeFusion and DistriFusion on A100 PCIe vs. NVLink cluster. (b) Latency of PipeFusion with various patch numbers  $M$  on 2, 4, 8 L20 GPUs for the task on three image generation resolutions.

### 4.2.3 Ablation Study

**Patch Number:** We analyze the impact of the setting of patch numbers  $M$  on PipeFusion as shown in Figure 10b. According to the analysis presented in Table 1, as  $M$  increases, memory consumption decreases, and there is no impact on communication. However, in practice,  $M$  should not be set too high. On tasks of 1024px and 2048px image generation, when  $M$  is beyond a certain threshold, the overall latency increases. However, such a phenomenon seldom exists on the higher resolution image 4Kx4K cases. This is because excessively fine-grained computation partitioning can lead to a decrease in the GPUs’ theoretical throughput.

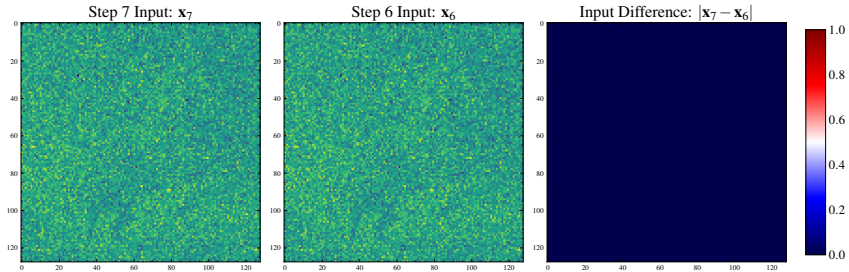
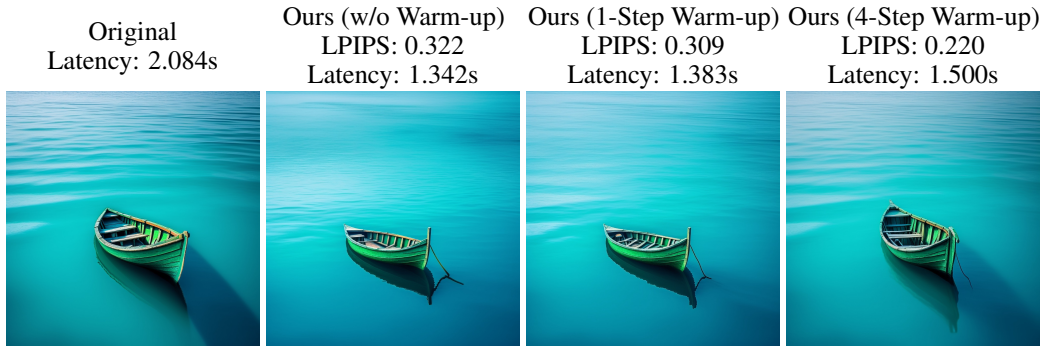


Figure 11: Visualization of the input from steps 6 and 7 and their difference of 1024px image generation using Pixar- $\alpha$ . All feature maps are channel-wise averaged. The difference is nearly all zero, which verifies the input temporal redundancy.

**Input similarity:** To verify the input temporal redundancy in DistriFusion [9], we also quantitatively calculate the model input difference across all consecutive steps. Figure 11 presents a qualitative visualization of the differences in input between step 7 and step 6. The results reveal that the variations between these inputs are minimal, with the vast majority of differences being negligible or approaching zero. This finding underscores the input temporal redundancy, that high degree of similarity between the input of consecutive steps within the diffusion process.

**Warmup Step:** the input temporal redundancy is relatively small in the initial few diffusion steps. Therefore, it is necessary to employ some warmup steps to use synchronous communication without resorting to stale activations, which would introduce waiting time, or bubbles, into the pipeline. As illustrated in Figure 12, when the warmup is set to 4, the 20-step DPM-solver produces images that are virtually indistinguishable from the original. However, without warmup or with a warmup of 1, the generated images clearly exhibit inferior quality compared to the original.

There are methods to mitigate the performance loss caused by the warmup steps. Firstly, our experiments involved a relatively small number of sampling steps, at 20. Increasing sampling steps, the overhead associated with warmup would diminish. Secondly, to mitigate the impact of warmup on latency, it can be executed on a separate device utilizing either sequence or tensor parallelism.



(a) Prompt: *A small boat in the blue and green water.*



(b) Prompt: *A motorcycle sits on the pavement on a cloudy day.*

Figure 12: Qualitative results on the 20-step DPM-Solver [18] with different warm-up steps and a patch number of 8. LPIPS is computed against the samples from the original PixArt- $\alpha$  [?] over the entire COCO [29] dataset. Adding the warm-up steps improves the performance while causing latency rise.

The computed results can then be transmitted to other devices for pipelined inference. Given the low computational proportion of warmup, it can be deployed with one dedicated warmup device alongside, for instance, ten computational devices.

## 5 Conclusion

This paper introduces PipeFusion to parallelize Diffusion Transformers (DiT) inference on multiple devices. By exploiting the input similarities across diffusion steps and employing a pipelined approach to orchestrate communication and computation, PipeFusion reduces both communication bandwidth and memory demands, making DiT inference more efficient on PCIe-connected devices. In the future, we plan to scale DiT inference to economical multi-node GPU clusters, utilizing PCIe for GPU interconnection within nodes and Ethernet for communication between nodes. We anticipate that PipeFusion will achieve even greater advantages in such environments.

## References

- [1] OpenAI. Video generation models as world simulators. <https://openai.com/index/video-generation-models-as-world-simulators/>, 2024. Accessed: May 2024.
- [2] Jiaming Song, Chenlin Meng, and Stefano Ermon. Denoising diffusion implicit models. *arXiv preprint arXiv:2010.02502*, 2020.
- [3] Olaf Ronneberger, Philipp Fischer, and Thomas Brox. U-net: Convolutional networks for biomedical image segmentation. In *Medical image computing and computer-assisted intervention—MICCAI 2015: 18th international conference, Munich, Germany, October 5-9, 2015, proceedings, part III 18*, pages 234–241. Springer, 2015.
- [4] William Peebles and Saining Xie. Scalable diffusion models with transformers. In *Proceedings of the IEEE/CVF International Conference on Computer Vision*, pages 4195–4205, 2023.

- [5] Mohammad Shoeybi, Mostofa Patwary, Raul Puri, Patrick LeGresley, Jared Casper, and Bryan Catanzaro. Megatron-lm: Training multi-billion parameter language models using model parallelism. *arXiv preprint arXiv:1909.08053*, 2019.
- [6] Sam Ade Jacobs, Masahiro Tanaka, Chengming Zhang, Minjia Zhang, Leon Song, Samyam Rajbhandari, and Yuxiong He. Deepspeed ulysses: System optimizations for enabling training of extreme long sequence transformer models. *arXiv preprint arXiv:2309.14509*, 2023.
- [7] Hao Liu, Matei Zaharia, and Pieter Abbeel. Ring attention with blockwise transformers for near-infinite context. *arXiv preprint arXiv:2310.01889*, 2023.
- [8] Andy Shih, Suneel Belkhale, Stefano Ermon, Dorsa Sadigh, and Nima Anari. Parallel sampling of diffusion models. *Advances in Neural Information Processing Systems*, 36, 2024.
- [9] MUYANG LI, Tianle Cai, JiAXIN CAO, QINSHENG ZHANG, Han Cai, Junjie Bai, Yangqing Jia, Ming-Yu Liu, Kai Li, and Song Han. Distrifusion: Distributed parallel inference for high-resolution diffusion models. In *Proceedings of the IEEE/CVF Conference on Computer Vision and Pattern Recognition (CVPR)*, 2024.
- [10] Dustin Podell, Zion English, Kyle Lacey, Andreas Blattmann, Tim Dockhorn, Jonas Müller, Joe Penna, and Robin Rombach. Sdxl: Improving latent diffusion models for high-resolution image synthesis. *arXiv preprint arXiv:2307.01952*, 2023.
- [11] Yanping Huang, Youlong Cheng, Ankur Bapna, Orhan Firat, Dehao Chen, Mia Chen, HyoukJoong Lee, Jiquan Ngiam, Quoc V Le, Yonghui Wu, et al. Gpipe: Efficient training of giant neural networks using pipeline parallelism. *Advances in neural information processing systems*, 32, 2019.
- [12] Deepak Narayanan, Aaron Harlap, Amar Phanishayee, Vivek Seshadri, Nikhil R Devanur, Gregory R Ganger, Phillip B Gibbons, and Matei Zaharia. Pipedream: generalized pipeline parallelism for dnn training. In *Proceedings of the 27th ACM symposium on operating systems principles*, pages 1–15, 2019.
- [13] Ziheng Jiang, Haibin Lin, Yinmin Zhong, Qi Huang, Yangrui Chen, Zhi Zhang, Yanghua Peng, Xiang Li, Cong Xie, Shibiao Nong, et al. Megascale: Scaling large language model training to more than 10,000 gpus. *arXiv preprint arXiv:2402.15627*, 2024.
- [14] Xin Ma, Yaohui Wang, Gengyun Jia, Xinyuan Chen, Ziwei Liu, Yuan-Fang Li, Cunjian Chen, and Yu Qiao. Latte: Latent diffusion transformer for video generation. *arXiv preprint arXiv:2401.03048*, 2024.
- [15] Arash Vahdat, Karsten Kreis, and Jan Kautz. Score-based generative modeling in latent space. *Advances in neural information processing systems*, 34:11287–11302, 2021.
- [16] Robin Rombach, Andreas Blattmann, Dominik Lorenz, Patrick Esser, and Björn Ommer. High-resolution image synthesis with latent diffusion models. In *Proceedings of the IEEE/CVF conference on computer vision and pattern recognition*, pages 10684–10695, 2022.
- [17] Yang Song, Jascha Sohl-Dickstein, Diederik P Kingma, Abhishek Kumar, Stefano Ermon, and Ben Poole. Score-based generative modeling through stochastic differential equations. *arXiv preprint arXiv:2011.13456*, 2020.
- [18] Cheng Lu, Yuhao Zhou, Fan Bao, Jianfei Chen, Chongxuan Li, and Jun Zhu. Dpm-solver: A fast ode solver for diffusion probabilistic model sampling in around 10 steps. *Advances in Neural Information Processing Systems*, 35:5775–5787, 2022.
- [19] Qinsheng Zhang and Yongxin Chen. Fast sampling of diffusion models with exponential integrator. *arXiv preprint arXiv:2204.13902*, 2022.
- [20] Qinsheng Zhang, Molei Tao, and Yongxin Chen. gddim: Generalized denoising diffusion implicit models. *arXiv preprint arXiv:2206.05564*, 2022.
- [21] Chenlin Meng, Robin Rombach, Ruiqi Gao, Diederik Kingma, Stefano Ermon, Jonathan Ho, and Tim Salimans. On distillation of guided diffusion models. In *Proceedings of the IEEE/CVF Conference on Computer Vision and Pattern Recognition*, pages 14297–14306, 2023.

- [22] Tim Salimans and Jonathan Ho. Progressive distillation for fast sampling of diffusion models. *arXiv preprint arXiv:2202.00512*, 2022.
- [23] Jiarui Fang and Shangchun Zhao. A unified sequence parallelism approach for long context generative ai. *arXiv preprint arXiv:2405.07719*, 2024.
- [24] Junsong Chen, Jincheng Yu, Chongjian Ge, Lewei Yao, Enze Xie, Yue Wu, Zhongdao Wang, James Kwok, Ping Luo, Huchuan Lu, et al. Pixart- $\alpha$ : Fast training of diffusion transformer for photorealistic text-to-image synthesis. *arXiv preprint arXiv:2310.00426*, 2023.
- [25] MIT-Han-Lab. Distrifuser. <https://github.com/mit-han-lab/distrifuser>, May 2024.
- [26] Xuanlei Zhao, Shenggan Cheng, Guangyang Lu, Jiarui Fang, Haotian Zhou, Bin Jia, Ziming Liu, and Yang You. Autochunk: Automated activation chunk for memory-efficient long sequence inference. *arXiv preprint arXiv:2401.10652*, 2024.
- [27] Hugging Face. Pixart-alpha model checkpoint. <https://huggingface.co/PixArt-alpha>, May 2024.
- [28] Martin Heusel, Hubert Ramsauer, Thomas Unterthiner, Bernhard Nessler, and Sepp Hochreiter. Gans trained by a two time-scale update rule converge to a local nash equilibrium. *Advances in neural information processing systems*, 30, 2017.
- [29] Xinlei Chen, Hao Fang, Tsung-Yi Lin, Ramakrishna Vedantam, Saurabh Gupta, Piotr Dollár, and C Lawrence Zitnick. Microsoft coco captions: Data collection and evaluation server. *arXiv preprint arXiv:1504.00325*, 2015.